15 December 2000

ELSEVIER

Chemical Physics Letters 332 (2000) 167–174

CHEMICAL PHYSICS LETTERS

www.elsevier.nl/locate/cplett

Trajectory calculations of two-dimensional Penning ionization electron spectra of N_2 in collision with metastable He^* 2^3S atoms

Koichi Ohno [a,*], Masakazu Yamazaki [a], Naoki Kishimoto [a], Tetsuji Ogawa [a], Kouichi Takeshita [b]

[a] *Department of Chemistry, Graduate School of Science, Tohoku University, Aramaki, Aoba-ku, Sendai 980-8578, Japan*
[b] *Tokyo University of Agriculture, Yasaka 196, Abashiri 099-2943, Japan*

Received 11 September 2000; in final form 6 October 2000

Abstract

Ionization cross-sections of N_2 in collision with He^* 2^3S as functions of the collision energy and the ejected electron kinetic energy (two-dimensional Penning ionization electron spectra, 2D-PIES) have been evaluated by trajectory calculations based on quantum chemical potential surfaces of both entrance and exit channels as well as on the transition widths for producing X, A, and B states of N_2^+. The present approach using a Li atom for He^* and an overlap approximation for Γ has given theoretical 2D-PIES in good agreement with the observation and a promise for its application to the study of dynamics in collisional ionization involving highly anisotropic target systems. © 2000 Elsevier Science B.V. All rights reserved.

1. Introduction

Since electron spectroscopic techniques [1–3] were applied to the Penning ionization, which occurs on collisions of metastable rare gas atoms Rg^* with atoms or molecules, collisional ionization dynamics have not been elucidated in detail for molecular targets. One of the major obstacles has been the difficulty to obtain experimental information on specified states of both reactants and products. Another obstacle has been the difficulty to reproduce the observed electron spectra in good quantitative accuracy by theoretical calculations.

In the measurements of the yield of Penning ions as functions of the collision energy E_c [4–6], ionic states of produced ions or kinetic energy of ejected electrons were disregarded. Although Penning ionization electron spectra (PIES) have been observed as functions of the kinetic energy E_e of ejected electrons [1], selection of collision energies has long been avoided except for a special case [7]. Experimental difficulties associated with simultaneous analyses of both E_c and E_e have been overcome by using a nozzle discharge beam [8–11] and a supersonic beam [12–14] for producing He^* atoms. These new techniques have made it possible to observe collision energy dependence of partial Penning ionization cross-sections (CEDPICS) [8–11] as well as collision-energy-resolved PIES (CERPIES) [11–14]. These two modes of experiment have recently been combined into a novel

* Corresponding author. Fax: +81-22-217-6580.
E-mail address: ohnok@qpcrkk.chem.tohoku.ac.jp (K. Ohno).

0009-2614/00/$ - see front matter
PII: S0009-2614(00)01240-9

technique observing two-dimensional PIES (2D-PIES) in which electron counting-rates are measured as functions of both E_c and E_e [15,16]. Recent studies of collision energy dependence of fragment species produced with the impact of Rg* have also provided novel information [17,18].

The fundamental theory of Penning ionization was established by Nakamura [19] and Miller [20]. Some aspects were numerically calculated in detail for simple targets, such as H [21,22] and H_2 [23,24], based on quantum chemical treatments. Semi-empirical potential functions have been applied to other target systems having many electrons, such as Ar [13,15] and N_2 [16]. Longley et al. [13] have made model potential calculations in comparison with the observed CERPIES of Ar with He* (2^1S). Ohno and coworkers [15] have calculated 2D-PIES in good agreement with the experiment for Ar in collision with He* 2^3S and He* 2^1S. Dunlavy and Siska [14] have reported simulations of CERPIES for N_2 with He* 2^1S. In these studies, employed potentials and ionization widths were empirical, and their functional forms were restricted. Such an empirical approach has an essential drawback becoming more difficult to describe anisotropies with the molecular size increasing.

In the present study, 2D-PIES of N_2 in collision with metastable He* 2^3S atoms as functions of E_c and E_e have been calculated by using entrance, exit, and imaginary potentials based on quantum chemical calculations with various levels of approximation and compared with the observation.

2. Construction of interaction potentials

2.1. Entrance potential between N_2 and He* 2^3S

Entrance potentials involving electronic excited states embedded in ionization continua are difficult to be determined. For N_2 and He* 2^3S, Ishida and Horime [25] performed calculations based on ab initio resonance potentials and ionization widths by using Feshbach projection operator method. Although qualitative features were found to be similar with the experiment, quantitative details were not satisfactory. Such an approach dealing with excited-state potentials is preferable, but the results are still disappointing.

It has been established that interaction potentials between Rg* and various targets can be approximated by replacing Rg* by the respective alkali atom with the same electron configuration in the valence shell [7,26]. On this basis, a Li 2^2S atom was used in place of a He* 2^3S atom for calculations of entrance potentials. The N–N distance was fixed at the experimental value of 1.0976 Å for N_2. Interaction energies were obtained by the coupled cluster method including singles, doubles and optional triple terms (CCSD(T)) with basis functions of 6-311 + G*. Full counterpoise corrections were made to avoid basis set superposition errors (BSSE) [27]. Polar grids were used to obtain the interaction energy at an arbitrary geometry; appropriate radial distances R of less than 10 points with respect to the center of mass of N_2 were sampled, and angles of 7–10 directions were selected. A cubic spline technique was used for both radial and angular directions to obtain interaction energies for arbitrary points. Rectangular grids were not employed because of the very slow convergence. Legendre expansions for anisotropic potentials were not used, since highly anisotropic nature might be disregarded.

Because of the approximate nature of the Li–N_2 potentials V_a, entrance potentials V_0 were estimated as $V_0 = cV_a$ with a scale factor c, which was determined to be 0.80 so as to reproduce observed CEDPICS. Obtained entrance potentials V_0 are shown in Fig. 1a for directions of 0° and 90° with respect to the N–N axis.

2.2. Exit potential between N_2^+ and He

Ionic states of N_2^+ produced by He* 2^3S are $X^2\Sigma_g$, $A^2\Pi_u$, and $B^2\Sigma_u$ states corresponding to ionization from $3\sigma_g$, $1\pi_u$, and $2\sigma_u$ molecular orbitals of N_2. Energies of the exit potentials $V_+^{(i)}$ for the ith ionic state of N_2^+ interacting with a ground-state He atom were calculated by several ways. The absolute value of an orbital energy can be treated as the respective ionization energy (IE). This method is referred to HF. The second method is the outer valence Green's function method (OVGF) in which many body effects are included

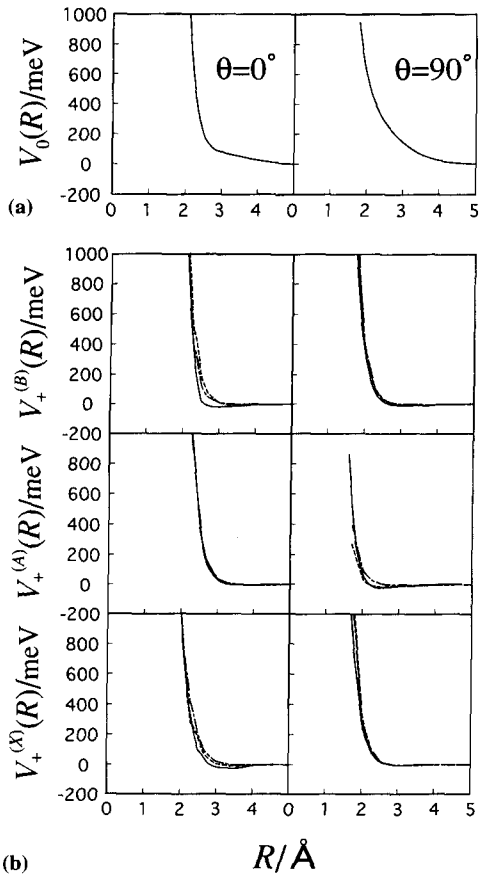

Fig. 1. Entrance and exit potentials for directions of 0° and 90° with respect to the N–N axis. R is the distance between the center of mass of N_2/N_2^+ and $He^*(Li)/He$: (a) Entrance potential curves $V_0(R)$. (b) Exit potential curves $V_+^{(i)}$ by the methods of HF (dash and dot), OVGF (dash), and MRSDCI (solid). X, A, and B are respective ionic states of N_2^+.

[28]. The third method is a method of multi-reference single and double excitation configuration interactions (MRSDCI). HF and OVGF calculations were made by a program of GAUSSIAN 94 with basis sets of 6-311+G* for N and 6-311++G** for He. MRSDCI calculations were performed by a program of ALCHEMY2 with a basis set of MIDI-4 + polarization. The N–N distance was fixed at 1.0976 Å, since ionization can be treated as adiabatic processes. Although selected geometries and data handlings were nearly the same as those for entrance potentials, no scaling factors were introduced. Since our interests are focused on the shape of potential energy surfaces rather than their absolute values, calculated IE's are only treated as the relative values with respect to the isolated molecular ion. Obtained exit potentials are shown in Fig. 1b. Vertical IE's for constructing 2D-PIES were taken from observed He I photoelectron spectrum of N_2 [29].

2.3. Imaginary potential (transition width)

The imaginary part of the entrance potential, $-i\Gamma/2$, is related to the ionization width $\Gamma^{(i)}$ for the ith ionic state, which is given by

$$\Gamma^{(i)} = 2\pi\rho^{(i)}\left|\langle\Phi_0|H_{el}|\Phi^{(i)}\rangle\right|^2. \quad (1)$$

Here, $\rho^{(i)}$ is the density of final states, H_{el} the electronic Hamiltonian, and Φ_0 and $\Phi^{(i)}$ are the electronic wave functions for the initial and the ith final states, respectively. In many studies, the dependence of $\Gamma^{(i)}$ on the distance R was assumed as $A\exp(-\alpha R)$ [2,13–15]. However, for molecular target systems both A and α are highly anisotropic in addition to extra R-dependence. Since matrix elements in Eq. (1) are essentially governed by mutual overlaps between orbitals of the interacting system [30], the following formula can be used:

$$\Gamma^{(i)} = K^{(i)}|\langle\phi_i \mid \psi_{1s}\rangle|^2. \quad (2)$$

Here, ϕ_i and ψ_{1s} are the ionized orbital corresponding to the ith ionic state and the He 1s orbital, respectively. $K^{(i)}$ were determined in order to reproduce the observed branching ratios and the experimental total ionization cross-section of 14 $Å^2$ at $E_c = 200$ meV [5]. Orbital functions were obtained from ab initio self-consistent field calculations for the isolated molecule and a He atom.

3. Calculations of 2D-PIES

3.1. Trajectory calculations

Classical trajectories were calculated on the basis of the entrance potential for a He^*/Li and N_2 treated as a rigid-rotor. The initial rotational energies were generated statistically so as to fit with the Boltzmann distribution at 300 K. Initial conditions for ca. 100 000 trajectories were generated as follows. E_c was set between 70 and 380 meV

with spacing of 10 meV. For a given E_c, 3000 trajectories were generated. Initial directions of incident He^* atom with respect to the orientation of N_2 and its rotational axis were randomly generated. The impact parameter b was set randomly from 0 to 7 Å. Differential equations were solved numerically by the fourth-order Runge–Kutta method with an adaptive step size control.

In a real trajectory, the ionization event occurs at most once at a certain position of that trajectory. For a bundle of the same trajectories, a survival factor S at a particular time t (or at a geometrical position) can be treated as the survival probability of He^* in the excited state. At the initial condition, $t = 0$ and $S = 1$. The partial ionization probability $P^{(i)}$ is also a function of time and positions, which can be determined by integration of transition probabilities $W^{(i)}$ into the ith ionic state before time t (or before arriving at the position). These quantities should satisfy the following differential equations:

$$dS/dt = -S\sum_i W^{(i)}, \tag{3}$$

$$dP^{(i)}/dt = SW^{(i)}. \tag{4}$$

Since $W^{(i)} = \Gamma^{(i)}/\hbar$, $P^{(i)}$ and S for a particular trajectory can be evaluated for only one span of the same trajectories. Dwelling time τ at a certain region in a trajectory was calculated from the relative velocity of the system. Thus, partial transition probabilities in a certain region in a trajectory were obtained as $SW^{(i)}\tau$.

3.2. Construction of 2D-PIES

2D-PIES were constructed as transition probabilities as functions of E_e and E_c, for three sets of exit potentials (HF, OVGF, and MRSDCI). For a given E_c, the distribution of transition probabilities as functions of E_e (CERPIES) was obtained as follows: (1) Values of E_e for three ionic states at each geometrical position on a trajectory were calculated by the energy difference of entrance and exit potentials, $V_0 - V_+^{(i)}$. The relative separations of entrance and exit potentials at the infinite distance were adapted to those corresponding to the observed IE's for He I UPS. Electron energy distribution functions $D(E_e)$ were then obtained from sets of values $(V_0 - V_+^{(i)}, SW^{(i)}\tau)$ by integrating such data for many trajectories at a given E_c. (2) Franck–Condon factors and vibrational intervals for N_2 were taken from studies on UPS [31]. Vibrational structures were constructed by redistributing $D(E_e)$. In this treatment, intramolecular potentials of the ion were assumed to be irrelevant with the existence of the He atom. (3) Apparatus functions with a width of 143 meV were used to redistribute the spectra of $D(E_e)$. (4) Calculated CERPIES were then converted into 2D-PIES by using a smoothing technique for the function of E_c.

4. Results and discussion

4.1. CEDPICS

Although computed CEDPICS for N_2 with He^* (2^3S) has been reported to be in good agreement with the observation [32], relative magnitudes of partial cross-sections (branching ratios) showed some discrepancies from the observed data [9,16]. In order to construct 2D-PIES, this has been a serious drawback. Since Eq. (2) is a compromise between rigorous treatments and efficiencies, the constant $K^{(i)}$ was adjusted for each ionic state in the present study; $K^{(X)} : K^{(A)} : K^{(B)} = 0.81 : 1.44 : 1.96$. Obtained CEDPICS are shown in Fig. 2. Computed results for both total and partial cross-sections are in good agreement with the experiment, although the lower energy parts are less satisfactory, which will be discussed below in connection with the quality of the computed entrance potential.

4.2. CERPIES and 2D-PIES

Fig. 3 shows CERPIES and 2D-PIES for N_2 with He^* 2^3S; Fig. 3a shows the observed 2D-PIES [16], and computed results by using HF, OVGF, and MRSDCI methods are shown in Fig. 3b, c, d, respectively. The following experimental features are well reproduced: (i) Intensities are increasing with the increase of E_c, especially more rapidly for the A state, in agreement with the observed behavior in CEDPICS. (ii) Peak positions slightly

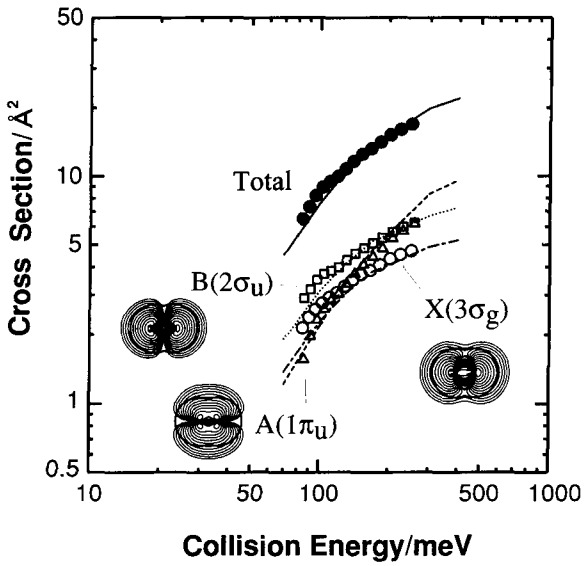

Fig. 2. Collision energy dependence of total and partial Penning ionization cross-sections for N_2/He^* (2^3S). Observed data are plotted by solid circle for total cross-sections, open circle, triangle, and square for partial cross-sections for producing X, A, and B states, respectively. Calculated data are plotted by solid line for the total cross-sections, dash-and-dot, dash, and dot lines for partial cross-sections for producing X, A, and B states, respectively. Electron density maps are also shown for the relevant molecular orbitals with an approximate repulsive surface by the solid curve.

shift toward the higher E_c with the increase of E_c. (iii) Band widths are increasing and extremely expanded to the higher E_e side with the increase of E_c.

For further analyses, peak positions of the most prominent vibrational peaks ($v = 0$ for X and B states, $v = 1$ for A state) in observed and calculated CERPIES are listed for $E_c = 100$ and 300 meV in Table 1. Full-widths at half-maxima are also listed for X and B states. Relative peak shifts on going from $E_c = 100$ to $E_c = 300$ meV were observed to be 0.04 eV (X), 0.06 eV (A), and 0.03 eV (B). Although calculated peak shifts are satisfactory, the absolute peak positions are significantly different among HF, OVGF, and MRSDCI. It is rather unbelievable that HF gave better agreement with the observation than MRSDCI. Since the electron energies E_e are related to the potential energy difference of $V_0 - V_+^{(i)}$ [2,3] the calculated values depend on the subtle balance between the entrance and exit potentials.

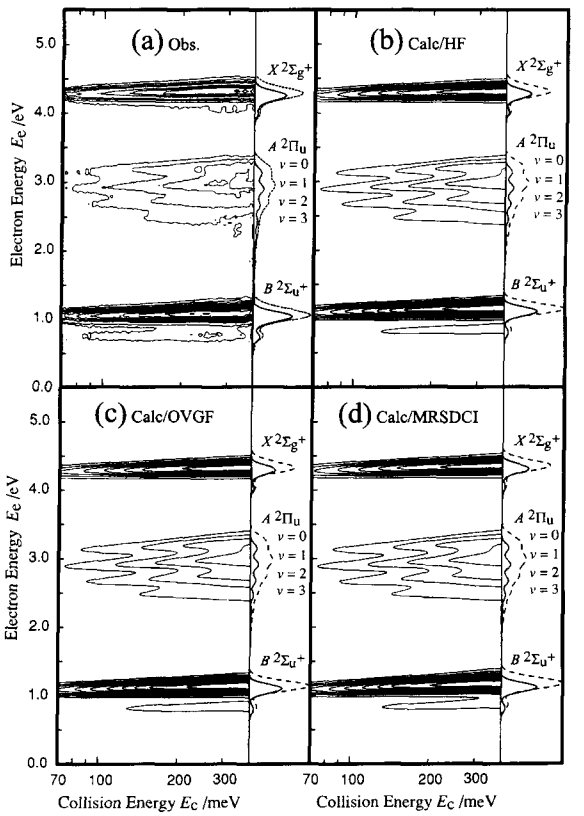

Fig. 3. 2D-PIES for N_2/He^* (2^3S). In the right-hand sides, CERPIES are also shown at $E_c = 100$ (solid) and 300 (dashed) meV with labels for ionic states of X, A, and B as well as vibrational labels for the A state: (a) Observed 2D-PIES (Ref. [16]). (b)–(d) are calculated 2D-PIES by the methods of HF (b), OVGF (c), and MRSDCI (d), respectively.

Table 1
Peak positions (eV) of the most prominent vibrational bands in CERPIES for $E_c = 100$ and 300 meV[a]

	E_c (meV)	$X^2\Sigma_g$	$A^2\Pi_u$	$B^2\Sigma_u$
Obsd.	100	4.26 (163)	2.90	1.04 (165)
	300	4.30 (200)	2.96	1.07 (203)
HF	100	4.28 (151)	2.91	1.10 (155)
	300	4.32 (182)	2.98	1.14 (180)
OVGF	100	4.29 (157)	2.91	1.11 (157)
	300	4.33 (177)	2.98	1.14 (182)
MRSDCI	100	4.31 (158)	2.91	1.12 (159)
	300	4.35 (187)	2.98	1.17 (199)

[a] Full-widths at half-maxima (meV) are also shown for X and B states in parentheses.

It should be stressed that the entrance potentials are very sensitive to the methods. It was pointed out that basis functions to describe the outer part of interacting systems are crucially important in addition to inclusion of polarization functions and electron correlation effects [32,33]. In Ishida's calculation [25], too much repulsive interactions in the long-range resulted in too small cross-sections, especially for the low E_c regions. This difficulty has been partly overcome by introducing a scaling factor and the use of diffuse basis functions [33]. However, as mentioned for the present result of computed CEDPICS, low energy sides of calculated cross-sections are found to be still smaller than the observation. In other words, calculated entrance potentials are rather higher than the real curves. This discrepancy may be due to the following factors, which possibly lead to reduction of potential energies by ca. 50 meV; (1) insufficient inclusion of electron correlation effects, and (2) the fixed bond length for the rigid-rotor.

On the other hand for the exit potentials, electron correlation effects seem to be not so crucial. HF and OVGF gave nearly the same exit potentials, which is also very similar to the case of MRSDCI. A little discernible difference among the exit potentials is that the curves for MRSDCI are slightly pulled down at the foot of the repulsive wall, which may lead to larger E_c of ca. 20–30 meV in the electron spectra with respect to those for OVGF and HF.

These features in the qualities of calculated potentials explain the unbelievable agreement of the absolute peak positions for HF and OVGF rather than MRSDCI. For the entrance potentials, correlation effects are underestimated to lead to larger E_c by ca. 50 meV, this is comparable to the unexpected overestimate of peak positions for MRSDCI. On the other hand, HF and OVGF underestimate correlation effects in the exit potentials by 20–30 meV may lead to the smaller discrepancies from the experiment.

The bandwidth being broadened with the increase of E_c is due to the repulsive wall of the entrance potential. With the increase of E_c, ionization probabilities at turning points on the repulsive wall become more efficient to result in generation of fast electrons. Calculated widths in Table 1 are in good agreement with the experiment for all three methods, since repulsive walls over than 100 meV are rather insensitive to electron correlation effects.

4.3. Non-Franck–Condon behaviors

Vibrational intervals of the observed ionization bands are in good agreement with the present calculations. This means that intramolecular potentials in ionic states are insensitive to the presence of the ground-state He atom. The observed vibrational intensity distribution for A state was found to be in good agreement with the calculated Franck–Condon pattern. While for X and B states, calculated intensity ratios for $I_{0\,1}/I_{0\,0}$ were found to be smaller than the observed values; when compared with the experiment, calculated ratios were reduced by a factor of 0.88–0.95 for X state, and by a factor of 0.64–0.67 for the B state. For the non-Franck–Condon behaviors, no E_c dependence could be found, although final-state dependence is marked due to the anisotropy of the interactions.

4.4. Remarks on the computations

Concerning with computational methods, some comments can be made. First of all, for the excited-state potential, the so-called 'peel-core' model has been used [14]. This model uses a switching function combining the core (He^+ + target) for the short range with the peel (He^* + target) for the long range. The angular dependence is introduced by the Legendre expansion containing the spherical and the second-order terms only, and the radial dependence has been treated empirically in terms of the modified Tang–Toennies van der Waals (TTVDW) forms composed of electrostatic interactions due to electric moments [34,35]. Serious problems of the core-peel method are summarized as follows: (1) In molecular systems, interactions are highly anisotropic, and thus the angular dependence up to the second-order terms may lead to considerable errors. (2) Expansions of radial parts in terms of TTVDW forms may also lead to serious errors, since quantum chemical interactions between molecular orbitals are not necessarily

described by simple electrostatic interactions of local electric moments. In order to avoid such difficulties, quantum chemical ab initio methods are preferable and more promising, since no assumptions of functional forms are included. Some care should of course be paid for the use of quantum chemical methods: (1) Suitable levels of diffuse functions should be included in the basis set to remove BSSE. (2) Inclusion of electron correlation effects should be made carefully to obtain sufficient accuracies. Present calculations of the entrance potentials indicate that quantum chemical calculations tend to underestimate electron correlation effects especially for the lower parts of the repulsive wall. The fixed bond length may also be a cause of the discrepancy for the entrance potential.

For the exit potentials, electron correlation effects are unexpectedly not so dramatic, as can be seen from the small difference among HF, OVGF, and MRSDCI in Fig. 3b,c,d. This is probably due to electrostatic interactions between a molecular ion and a neutral He atom being dominant. It should be noted that the exit potentials for X and B states are significantly different for the collinear direction ($\theta = 0°$), although Dunlavy and Siska assumed these to be the same [14]. The special reactivity for producing the B state can be related with the larger $K^{(i)}$ value and the more non-Franck–Condon behavior of vibrational bands for the B state in comparison with those for the X state. Provable reason for this may be the energy gap between the target orbital and He 1s orbital being the smallest for the $2\sigma_u$ orbital.

5. Concluding remarks

The present study demonstrates that the quantum chemical approach using ab initio wave functions rather than assuming traditional forms of both real and imaginary parts of potentials are promising for prediction as well as analyses and interpretation of collisional ionization processes. The present approach using a Li atom for He^* as well as an overlap approximation for Γ to avoid computational difficulties was found to be satisfactory. The advantage of the quantum chemical approach is the automatic inclusion of details of anisotropic characteristics for molecular targets, while for the assumed radial functions along with the Legendre expansion many features tend to be disregarded.

References

[1] V. Čermák, J. Chem. Phys. 44 (1966) 3781.
[2] A. Niehaus, Adv. Chem. Phys. 45 (1981) 399.
[3] A.J. Yencha, in: C.R. Brundle, A.D. Baker (Eds.), Electron Spectroscopy: Theory, Techniques and Applications, vol. 5, Academic Press, New York, 1984.
[4] E. Illenberger, A. Niehaus, Z. Phys. B 20 (1975) 33.
[5] T.P. Parr, D.M. Parr, R.M. Martin, J. Chem. Phys. 76 (1982) 316.
[6] L. Appolloni, B. Brunetti, J. Hermanussen, F. Vecchiocattivi, G.G. Volpi, J. Chem. Phys. 87 (1987) 3804.
[7] H. Hotop, Radiat. Res. 59 (1974) 379.
[8] K. Mitsuke, T. Takami, K. Ohno, J. Chem. Phys. 91 (1989) 1618.
[9] K. Ohno, T. Takami, K. Mitsuke, T. Ishida, J. Chem. Phys. 94 (1991) 2675.
[10] T. Takami, K. Mituske, K. Ohno, J. Chem. Phys. 95 (1991) 918.
[11] T. Takami, K. Ohno, J. Chem. Phys. 96 (1992) 6523.
[12] D.C. Dunlavy, D.W. Martin, P.E. Siska, J. Chem. Phys. 93 (1990) 5347.
[13] E.J. Longley, D.C. Dunlavy, M.F. Falcetta, H.M. Bevsek, P.E. Siska, J. Phys. Chem. 97 (1993) 2097.
[14] D.C. Dunlavy, P.E. Siska, J. Phys. Chem. 100 (1996) 21.
[15] K. Ohno, H. Yamakado, T. Ogawa, T. Yamata, J. Chem. Phys. 105 (1996) 7536.
[16] N. Kishimoto, M. Fruhashi, K. Ohno, J. Elec. Spectros. Relat. Phenom. 88–91 (1998) 143.
[17] I. Tokue, Y. Sakai, K. Yamasaki, J. Chem. Phys. 106 (1997) 4491.
[18] B. Brunetti, P. Candori, J. De Andres, F. Pirani, M. Rosi, S. Falcinelli, F. Vecchiocattivi, J. Phys. Chem. A 101 (1997) 7505.
[19] H. Nakamura, J. Phys. Soc. Jpn. 26 (1969) 1473.
[20] W.H. Miller, J. Chem. Phys. 52 (1970) 3563.
[21] W.H. Miller, H.F. Schaefer III, J. Chem. Phys. 53 (1970) 1421.
[22] M. Movre, W. Meyer, J. Chem. Phys. 106 (1997) 7139.
[23] J.S. Cohen, N.F. Lane, J. Chem. Phys. 66 (1977) 586.
[24] A.P Hickman, A.D. Issacson, W.H. Miller, J. Chem. Phys. 66 (1977) 1483.
[25] T. Ishida, K. Horime, J. Chem. Phys. 105 (1996) 5380.
[26] H. Haberland, Y.T. Lee, P.E. Siska, Adv. Chem. Phys. 45 (1981) 487.
[27] S.F. Boys, F. Bernardi, Mol. Phys. 19 (1970) 553.
[28] J.V. Ortiz, J. Chem. Phys. 104 (1996) 7599.
[29] K. Kimura, S. Katsumata, Y. Achiba, T. Yamazaki, S. Iwata, Handbook of He I Photoelectron Spectra of

Fundamental Organic Molecules, Japan Scientific, Tokyo, 1981.
[30] H. Hotop, A. Niehaus, Z. Phys. 228 (1969) 68.
[31] T.H. Lee, J.W. Rabalais, J. Chem. Phys. 61 (1974) 2747.
[32] K. Ohno, S. Sunada, Proc. Ind. Acad. Sci. 106 (1994) 327.
[33] T. Ogawa, K. Ohno, J. Chem. Phys. 110 (1999) 3773.
[34] K.T. Tang, J.P. Toennies, J. Chem. Phys. 80 (1984) 3726.
[35] P.E. Siska, J. Chem. Phys. 85 (1986) 7497.